Technical University of Denmark

DTU

Entropy generation minimization of one and two-stage tube in tube ammonia evaporators cooling high pressure gaseous hydrogen for vehicle refuelling

Jensen, Jonas Kjær; Rothuizen, Erasmus Damgaard; Markussen, Wiebke Brix

DTU Library
Technical Information Center of Denmark

Entropy generation minimization of one and two-stage tube in tube ammonia evaporators cooling high pressure gaseous hydrogen for vehicle refuelling

Jonas K. Jensen[a], Erasmus D. Rothuizen[b] and Wiebke B. Markussen[c]

[a] Technical University of Denmark, Kgs. Lyngby, Denmark, jkjje@mek.dtu.dk, CA
[b] Technical University of Denmark, Kgs. Lyngby, Denmark, edro@mek.dtu.dk
[c] Technical University of Denmark, Kgs. Lyngby, Denmark, wb@mek.dtu.dk

Abstract:

Gaseous hydrogen as an automotive fuel is reaching the point of commercial introduction. To facilitate this coming fleet of hydrogen vehicles, refuelling stations must be implemented. To ensure a costumer acceptable refuelling duration without overheating the vehicle's hydrogen tank, hydrogen must be supplied at a temperature of -40°C. This paper presents a study on the design of coaxial tube in tube ammonia evaporators for three different concepts of hydrogen cooling, one one-stage and two two-stage. A multi objective optimization has been imposed to minimize the entropy generation rate and evaporator size. For the two-stage concepts, the optimal intermediate temperatures have been found by minimizing the thermally driven entropy generation rate. A zero-dimensional numerical heat transfer model of the tube in tube evaporator is developed in Engineer Equation Solver using heat transfer and pressure drop correlations from the open literature. With this heat transfer model the optimal choice of tube sizes and circuit number is found for all three concepts. The results showed that cooling with a two-stage evaporator after the pressure reduction of hydrogen yields the lowest entropy generation rate, 49% lower than the highest, which was encountered with an one-stage evaporator after the pressure reduction. This entropy generation reduction requires an increase in evaporator size of 59% compared to the one-stage cooling. Two-stage cooling with the high-stage before the pressure reduction and the low-stage after, resulted in a 42% reduction of entropy generation but equally 59% of evaporator size increase.

Key Words:

Entropy generation minimization, Evaporator design, Heat transfer modelling, Hydrogen refuelling, Refrigeration

1 Introduction
1.1 Background

The issues of fossil fuel depletion and carbon-dioxide emissions are some of the main factors for assessing energy carriers for private transport. A transition from fossil fuels to renewable and zero emission energy carriers is a requirement for the development of a future sustainable transport sector. Introducing hydrogen as an energy carrier for private transportation is one measure for addressing these issues. Recent years research and development in gaseous hydrogen fuel cell vehicles, has matured the technology to a point of commercial introduction. To facilitate this coming fleet of hydrogen vehicles, a hydrogen infrastructure and consequently, hydrogen refuelling stations must be implemented. The development of hydrogen refuelling stations is torn between two often opposing objectives. Low energy consumption and high costumer acceptance. The first to comply with the sustainability aspect, the second to compete with conventional petrol or diesel refuelling.
Hydrogen vehicles attain a tank pressure of 70MPa after a refuelling by connecting the tank to a hydrogen bank of 90MPa. To regulate the refuelling duration an actuated pressure reduction valve is

placed in the hydrogen dispenser. This valve maintains a linear pressure increase in the vehicle's hydrogen tank. The slope of the pressure increase is termed the average pressure ramp rate (APRR) and the reduction valve the APRR-valve. To compete with conventional refuelling the duration must be as short as possible. Conversely, a too short refuelling duration causes tank overheat. The tank is heated by the sum of three phenomenons[1][2]. The heat of compression, the conversion of kinetic to internal energy and the negative Joule-Thomson coefficient of hydrogen. The negative Joule-Thomson coefficient causes a temperature increase of hydrogen when subjected to a forced adiabatic expansion, as in the APRR-valve. The dominating contribution to the tank heating is the heat of compression[3] and the conversion of kinetic to internal energy[1][2].

The refuelling duration can be reduced without overheating the hydrogen tank by cooling the hydrogen before it enters the vehicle[4]. The relation between refuelling duration and cooling temperature is given by SAE-J2601[5]. For hydrogen vehicles with tank capacities of 1-7kg a cooling temperature of -40°C is advised. To reduce the energy consumption required to attain this, the refrigeration system should be designed to minimize the exergy destruction within it. A reduction of exergy destruction in a vapour compression refrigeration system is best achieved by improving the evaporator as the endogenous avoidable exergy destruction here is the highest[6].

The choice of evaporator design is highly influenced by the pressure of upto 90MPa in the hydrogen supply system. This omits the application of typical designs such brazed plate or plate and shell. It is a general assumption that all hydrogen bearing passages must be composed of high pressure pipes. The coaxial tube in tube evaporator is capable of design for these restrictions and is therefore chosen. Due to the Joule-Thomson effect the evaporator must be placed as close to the dispenser nozzle as possible[5]. Thus the evaporator is to be built into the hydrogen dispenser introducing the size as constraint parameter. It is therefore not sufficient to design the evaporator for minimum entropy generation. The design must also minimize the evaporator size.

Ammonia is chosen as the refrigerant as it has no ozone depletion potential and a global warming potential >1[7]. Further ammonia has good thermophysical properties at the desired operating range.

1.2 Scope

This paper will study the design of evaporators for three different concepts of hydrogen cooling. Concept 1 is a one-stage evaporator after the APRR-valve, 2 is a two-stage evaporator after the APRR-valve and 3 is a two-stage evaporator with the high-stage before the APRR-valve and the low-stage after. All evaporators will be flooded coaxial tube in tube ammonia evaporators. The hydrogen and refrigerant pipe sizes included in this study will all be commercially available.

A zero-dimensional numerical heat transfer model of the tube in tube evaporator will be developed using heat transfer and pressure drop correlations from the open literature. The high-stage evaporation temperatures for concept 2 and 3 will be found by a minimization of the thermally driven entropy generation rate. With these optimal high-stage temperatures all combination of tube sizes and number of circuits are evaluated using the developed model. This will result in a range of feasible solution. An optimal solution for all three concepts will be sought. The optimal solution will be defined as the solution that provides the best trade-off between size and irreversibilities. Based on these optimal solutions the three cooling concepts will be compared.

1.3 System Description

1.3.1 Load and temperature levels

For a refuelling that complies with SAE-J2601 the peak cooling load is found for a refuelling with an ambient temperature of 30°C and an initial tank pressure of 2MPa. Under these conditions the refuelling duration is 150s[5]. The peak cooling load occurs approximately half way through the refuelling and is 72kW[8]. At the peak load the hydrogen mass flow rate is 0.05kg/s and the vehicles

hydrogen tank pressure is 36.5MPa[8]. The hydrogen bank temperature and pressure is assumed constant at 30°C and 90MPa respectively. These values are used as the dimensioning conditions for all three concepts.

1.3.2 Cooling Concept 1

Concept 1 utilizes one evaporative cold stream. The principal layout can be seen in figure 1a. As seen, one hydrogen cooling heat exchanger is placed between the APRR-valve and the nozzle. Thus this heat exchanger must cool all supplied hydrogen to the target temperature of -40°C and hence T_{evap} >-40°C. Figure 1b shows a $\dot{Q}$-T diagram of this cooling process. As seen a large ΔT exists in the first part of the evaporator. This ideally implies a small heat transfer area but also a high rate of entropy generation.
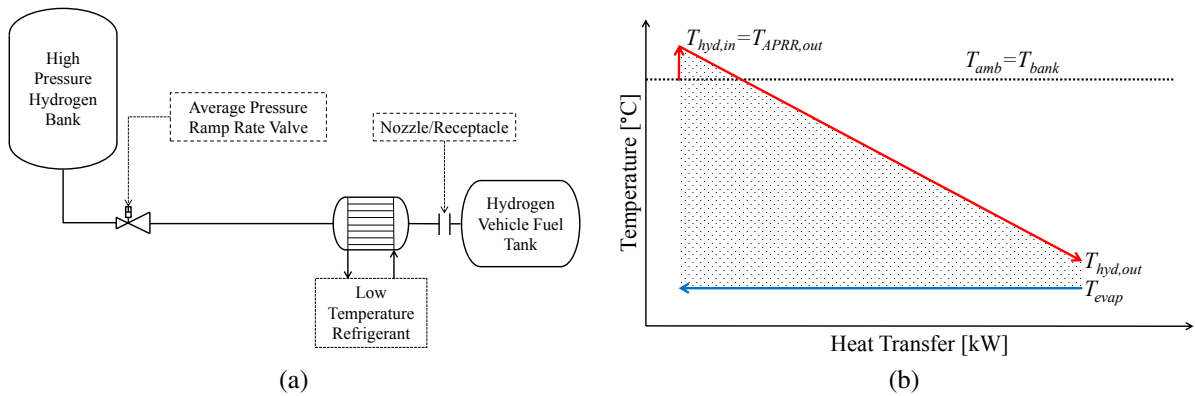

Fig. 1. (a) PID og hydrogen cooling concept 1. (b) $\dot{Q}$-T diagram of hydrogen cooling concept 1

1.3.3 Cooling Concept 2

Concept 2 utilizes two evaporative streams to cool the supplied hydrogen. The principal layout can be seen in figure 2a. As seen two hydrogen cooling heat exchangers are placed between the APRR-valve outlet and the nozzle.

A $\dot{Q}$-T diagram of this cooling process is shown in figure 2b. It is seen that the load share between the two heat exchangers is dependent on $T_{evap,H}$. Lowering $T_{evap,H}$ shifts load from the low to the high-stage and vice versa. Introducing a second evaporation stage gives the possibility of decreasing the entropy generation rate, compared to the one-stage concept, as the temperature gap between the hydrogen and the refrigerant can be reduced. This will consequently imply a larger heat transfer area.
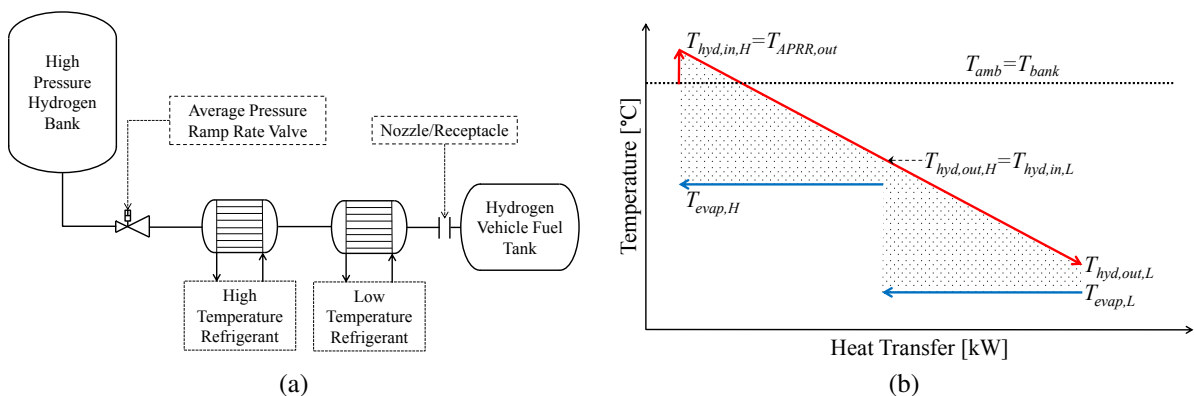

Fig. 2. (a) PID of hydrogen cooling concept 2. (b) $\dot{Q}$-T diagram of hydrogen cooling concept 2

1.3.4 Cooling Concept 3

Concept 3 equally utilizes two evaporative cold streams but has the high-stage situated upstream of the APRR-valve, see figure 3a. Hence the hydrogen is cooled prior to the adiabatic expansion in the

APRR-valve. The offset for the temperature increase induced by the Joule-Thomson effect is lowered in this case. The $\dot{Q}$-T plot is seen in figure 3b. As seen the temperature is first lowered from the hydrogen bank temperature, then throttled in the APRR-valve, resulting in an adiabatic temperature increase and then cooled to the target temperature of -40°C. Again this leads to a potential for entropy generation reduction, at the expense of a increased heat transfer area.

The main advantage of concept 3 compared to concept 2 is that the high-stage evaporator does not have to be placed in the dispenser unit. This will allow part of the increased heat transfer area, needed to reduce the entropy generation, to be placed in the hydrogen storage and process facility where the spatial constraints are not as rigorous.
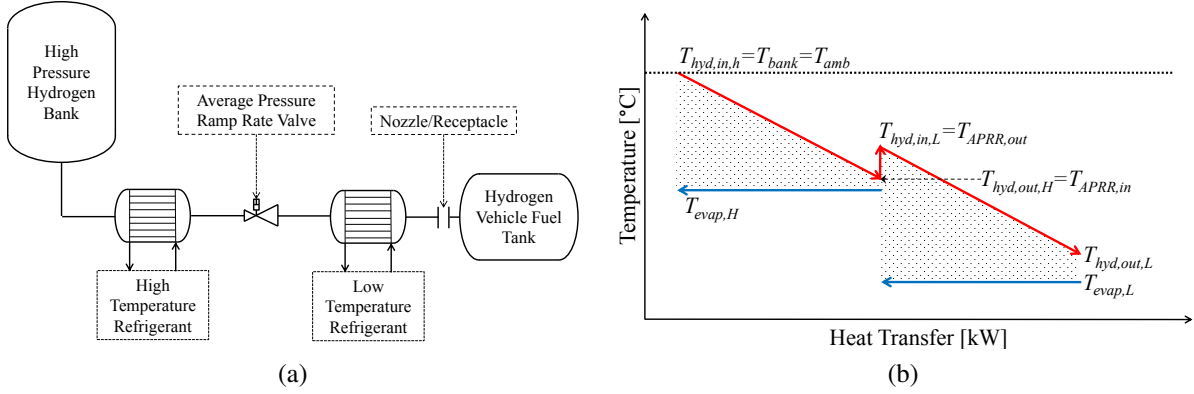

Fig. 3. (a) PID of hydrogen cooling concept 3. (b) $\dot{Q}$-T diagram of hydrogen cooling concept 3

2 Method
2.1 Optimal intermediate hydrogen temperature

For cooling concept 2 and 3 the thermally driven entropy generation rate is linked to the intermediate temperature of the hydrogen $T_{hyd,out,H}$, see figure 2a and 3a. Assuming a constant pinch temperature difference of 5°C on both the high and low-stage fixes the low-stage temperature to $T_{evap,L} = -45$°C and the high-stage temperature to $T_{evap,H} = T_{hyd,out,H} - 5$°C.

It is of interest to evaluate how the thermally driven entropy generation rate is related to the intermediate hydrogen temperature. If this can be quantified the optimal choice of intermediate temperature can be found.

To do this the thermally driven entropy generation rate is calculated on each of the evaporator stages using (1)[9]. Here $T_{hyd,avg}$ and $T_{ref,avg}$ are the thermodynamic average temperatures for the hydrogen stream and refrigerant stream respectively. The definition of thermodynamic average temperature can be seen in (2)[9]. These assume constant pressure. Assuming there is no superheat in the refrigerant stream the thermodynamic average temperature is equal to the evaporation temperature.

$$\dot{\Gamma}_s^T = \dot{Q}\frac{T_{hyd,avg} - T_{ref,avg}}{T_{hyd,avg}T_{ref,avg}} \qquad (1)$$

$$T_{avg} = \frac{h_{out} - h_{in}}{s_{out} - s_{in}} \qquad (2)$$

Using (1) and (2) along with energy and mass balance equations and an assumption of isenthalpic expansion in the APRR-valve, a parameter variation study of $T_{hyd,out,H}$ is performed in Engineering Equation Solver (EES)[10].
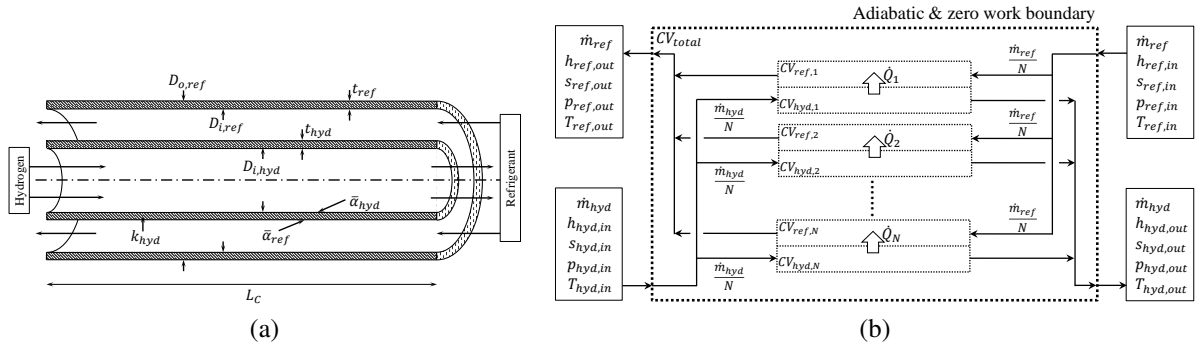
Fig. 4. (a) Principle sketch of one circuit of the coaxial tube in tube evaporator coil. (b) Control volume diagram for the heat transfer model of the coaxial tube in tube evaporator

2.2 Numerical heat transfer model of tube in tube evaporator

2.2.1 General assumptions

A principal sketch of the evaporator design can be seen in figure 4a. As seen this is a counterflow heat exchanger with the hydrogen flow in the inner tube and the two phase refrigerant flow in the annulus. The heat exchanger can be composed by a number of tube in tube pipes in a parallel connection, these will be referred to as circuits.

The objective of the model is to determine the length and entropy generation rate of the evaporator using different hydrogen and refrigerant pipe sizes as well as different numbers of circuits. The heat transfer model is developed in EES.

The general assumption are seen below:

- Steady state.
- No heat ingress from ambient.
- Constant heat flux on refrigerant side.
- Constant wall temperature on hydrogen side.
- Ideal distribution of hydrogen and refrigerant between evaporator circuits.
- Horizontal tubes.
- Inlet refrigerant vapour quality $x_i = 0$
- Outlet refrigerant vapour quality $x_o = 0.25$

2.2.2 Control volume definition and governing equation

The model consists of a number of control volumes as seen in figure 4. The control volume CV_{tot} surrounds the entire evaporator and calculates the total heat load and overall heat transfer coefficient UA. CV_{tot} has an adiabatic and zero work boundary thus there is assumed no losses to the environment. The control volumes $CV_{ref,1..N}$ surround the refrigerant flow in each of the circuits. These calculate the average heat transfer coefficient and the pressure drop of the refrigerant. $CV_{hyd,1..N}$ surrounds the hydrogen flow of each of the circuits and calculates the average heat transfer coefficient and the pressure drop of the hydrogen. Control volumes $CV_{ref,1..N}$ and $CV_{hyd,1..N}$ exchange only heat i.e no exchange of work or mass. The heat exchange rate relation is derived by applying a first law energy balance to CV_{tot}. This is seen in (3). The needed UA value is determined using (4) which is derived by combining Newtons law of convective cooling with the logarithmic mean temperature difference. The relationship between the needed circuit length and the average heat transfer coefficient is given in (5). The total entropy generation rate, with contribution from both thermal and pressure driven sources, is calculated by imposing an entropy balance on CV_{tot}, (6). Following the entropy generation is split into a thermally and pressure driven part. The pressure driven part is seen in (7). Here the subscript M implies the state (T_{amb}, p). Equation (7) is derived from spitting the physical exergy into thermal and mechanical parts and imposing an exergy balance to determine the thermal and mechanical exergy destruction. The Gouy-Stodola theorem is used convert the exergy destruction into entropy generation rates. The thermally driven part is found as the difference of the total and pressure

driven entropy generation.

$$\dot{Q} = \dot{m}_{hyd}\left(h_{hyd,in} - h_{hyd,out}\right) = \dot{m}_{ref}\left(h_{ref,out} - h_{ref,in}\right) \tag{3}$$

$$T_{hyd,out} = T_{ref,in} + \left(T_{hyd,in} - \bar{T}_{ref}\right)\exp\left(-\frac{UA}{\dot{m}_{hyd}c_{p,hyd}}\right) \tag{4}$$

$$UA = \left(\frac{1}{\bar{\alpha}_{hyd}2\pi D_{i,hyd}L_cN} + \frac{ln\left(\frac{D_{o,hyd}}{D_{i,hyd}}\right)}{k_{hyd}2\pi L_cN} + \frac{1}{\bar{\alpha}_{ref}2\pi D_{o,hyd}L_cN}\right)^{-1} \tag{5}$$

$$\dot{\Gamma}_s = \dot{m}_{hyd}\left(s_{hyd,out} - s_{hyd,in}\right) + \dot{m}_{ref}\left(s_{ref,out} - s_{ref,in}\right) \tag{6}$$

$$\dot{\Gamma}_s^P = \dot{m}_{hyd}\left(\frac{h_{hyd,in,M} - h_{hyd,out,M}}{T_{amb}} + \left(s_{hyd,in,M} - s_{hyd,out,M}\right)\right) + $$
$$\dot{m}_{ref}\left(\frac{h_{ref,in,M} - h_{ref,out,M}}{T_{amb}} + \left(s_{ref,in,M} - s_{ref,out,M}\right)\right) \tag{7}$$

$$\dot{\Gamma}_s^T = \dot{\Gamma}_s - \dot{\Gamma}_s^P \tag{8}$$

2.2.3   Heat transfer and pressure drop correlations

Table 1 states the used correlations sorted by media and flow type. As seen Shah's correlation[11] is used to predict local heat transfer coefficient for the two-phase ammonia flow. Contributions from both convective and nucleate boiling are accounted. The local heat transfer coefficient is evaluated for discreet values of vapour quality in the given range and then integrated to find the average. The hydraulic diameter of the annulus is used to correct for the non circular duct of the annulus.

The pressure drop in the two-phase ammonia is calculated as the sum of frictional and momentum pressure drop as described by Didi[12]. Here the pressure gradient is calculated using the Müller-Steinhagen and Heck's correlation[13].

For laminar hydrogen flow, Reynold's number <2300, the average heat transfer coefficient and pressure loss is calculated using correlations developed by Shah and London[14]. For turbulent flow, Reynold's number >5000, the average heat transfer coefficient is calculated using the Chilton-Colburn analogy[15] with the Churchill friction factor[16]. The pressure drop is calculated using Zigrang and Sylvester[17]. Heat transfer coefficents and pressure drops in the laminar to turbulent transition range, Reynold's number between 2300-5000, are calculated by interpolating between the laminar and turbulent correlations. The heat transfer correlation applied to hydrogen all assume simultaneously developing hydrodynamic and thermal flow. The effect of developing flow is accounted for by multiplying a factor related to the length to diameter ratio.

Table 1. Applied heat transfer and pressure drop correlations sorted by media and flow types.

Type	Media	Flow type	Correlation
Heat transfer	Ammonia	two-phase	Shah[11]
coefficient	Hydrogen	laminar	Shah & London[14]
	Hydrogen	turbulent	Chilton-Colburn[15], Churchill[16]
Pressure drop	Ammonia	two-phase	Muller-Steinhagen & Heck[13], Ould[12]
	Hydrogen	laminar	Shah & London[14]
	Hydrogen	turbulent	Zigrang and Sylvester[17]

2.2.4 Pipe sizes and material data

Table 2 shows the dimensions of the studied hydrogen and refrigerant pipes. The refrigerant pipes are all nominal pipe size (NPS), schedule 5[18]. The hydrogen pipes are commercial high pressure pipes approved for pressures upto 130MPa. All pipes are produced in stainless steel, thus the thermal conductivity is assumed to be the same. The value is set to $k = 0.016$kW/m-k. Likewise, the absolute roughness is assumed to be the same for all pipes and is set to a value of $\epsilon = 9 \cdot 10^{-5}$m.

Table 2. Inner and outer diameter and pipe wall thickness of studied refrigerant and hydrogen pipes.

	Hydrogen				Refrigerant		
NPS	D_o[mm]	t[mm]	D_i[mm]	NPS	D_o[mm]	t[mm]	D_i[mm]
DN32	42.16	1.651	38.858	DN6	6.350	1.790	2.770
DN40	48.26	1.651	44.958	DN10	9.530	2.180	5.170
DN50	60.33	1.651	57.028	DN15	14.29	3.180	7.930
DN65	73.03	2.108	68.814	DN20	19.05	3.960	11.13
DN80	88.90	2.108	84.684	DN25	25.40	5.570	14.27

3 Results

3.1 Optimal intermediate hydrogen temperature

Figure 5a shows the variation in thermal entropy generation and intermediate hydrogen temperature as a function of the load-share on the high-stage evaporator. The load-share is defined as $LS = \dot{Q}_H / \dot{Q}$. Hence for $LS = 0$ all load is delivered by the low-stage evaporator and concept 2 and 3 coincide with concept 1. For $LS = 1$ all load is delivered by the high-stage evaporator, for concept 2 this again coincides with concept 1. For concept 3 to have all load on the high-stage evaporator forces the high-stage outlet temperature to be -70°C in order for the temperature out of the APRR-valve to attain the target temperature of -40°C. It is also seen that for $LS > 0.75$ the high-stage evaporator for concept 3 is in principle the low-stage as $T_{evap,H} < T_{evap,L}$.

As seen in figure 5a the entropy generation rate is highly influenced by the choice of load share and subsequently intermediate hydrogen temperature. It is seen that the entropy generation rate decreases when increasing the load-share from 0→0.55 for concept 2 and for 0→0.49 for concept 3. Increasing the load share beyond these intervals causes the entropy generation rate to increase again. Hence the
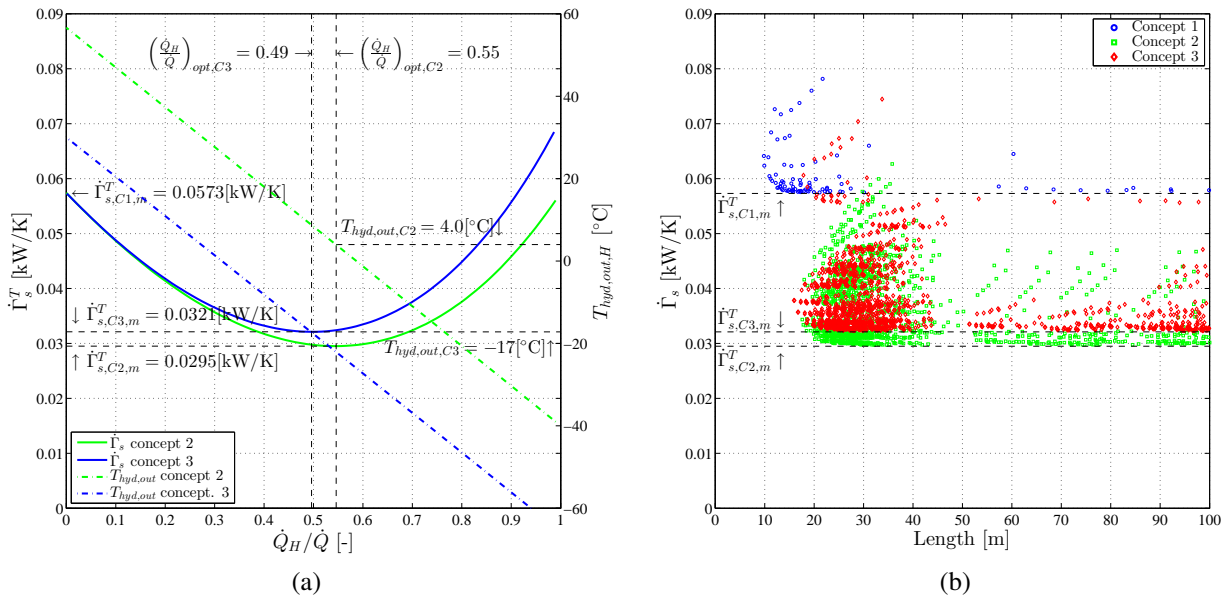

Fig. 5. (a) Entropy generation rate and intermediate hydrogen temperature as a function of the high-stage load-share for concepts 2 and 3. (b) Entropy generation rate and total tube length for all feasible solution of concept 1, 2 and 3

optimal load share for concept 2 is $LS_{opt,C2}$ =0.55 and $LS_{opt,C3}$ =0.49 for concept 3. This corresponds to a intermediate hydrogen temperature of 4°C for concept 2 and -17°C for concept 3.

At these intermediate hydrogen temperatures the thermal entropy generation rate is reduced to $\dot{\Gamma}_{s,C2}^{T}$ = 0.0295kW/K for concept 2 and $\dot{\Gamma}_{s,C3}^{T}$ =0.0321kW/K for concept 3. The thermal entropy generation rate for concept 1 is $\dot{\Gamma}_{s,C1}^{T}$ =0.0573kW/K. Hence at the optimal point concept 2 yields thermal entropy generation rate by 51%, lower than concept 1. For Concept 3 this value is 56%.

3.2 Optimal tube size combination and number of parallel circuits

Using the optimal intermediate temperatures derived from the minimization of the thermal entropy generation the optimal combination of hydrogen and refrigerant pipe size has been found along with the optimal number of circuits. The optimal solution is the combination that ensures the best trade off between the total entropy generation rate and the total length of tube needed to design the evaporator. The total length is defined as the length of one circuit multiplied by the number of circuits, $L = L_c \cdot N$. To evaluate this the heat transfer model of the tube in tube evaporator has been run for all combinations of the pipe sizes seen in table 2. Further this was combined with circuits numbers from 1 to 5.

Figure 5b shows the total length and entropy generation rate for all feasible solution for concept 1, 2 and 3. It can be seen that the feasible solutions for all three concepts each form a pareto frontier converging towards a minimum entropy generation rate in the horizontal direction and a minimum total length in the vertical direction. For concept 1 the minimum total length is L_m=10.8m and the minimum entropy generation rate is $\dot{\Gamma}_{s,m}$ =0.0574kW/K. For concept 2 the minimum total length is L_m=17.6m and the minimum entropy generation rate is $\dot{\Gamma}_{s,m}$ =0.0296kW/K. For concept 3 the minimum total length is L_m=17.6m and the minimum entropy generation rate is $\dot{\Gamma}_{s,m}$ =0.0322kW/K. All solutions on the pareto frontier are said to be pareto efficient solution and would be viewed as equally optimal in traditional optimization context. The usual method to find the global optimum would be to affiliate values as e.g. cost to the objectives of the optimization. Since this study seek only to find an appropriate trade off, the global optimum will be defined differently. The optimal solution will in this study be defined as the solution on the pareto frontier that has the shortest distance to the point$\left(L_m, \dot{\Gamma}_{s,m}\right)$.

Figure 6 and 6b shows the thermally and pressure driven entropy generation rate and total length for all the feasible solutions. It is seen that for all sizes the main contribution to entropy generation is the thermally driven contribution. Further it can be seen that the thermal part is highest for concept 1
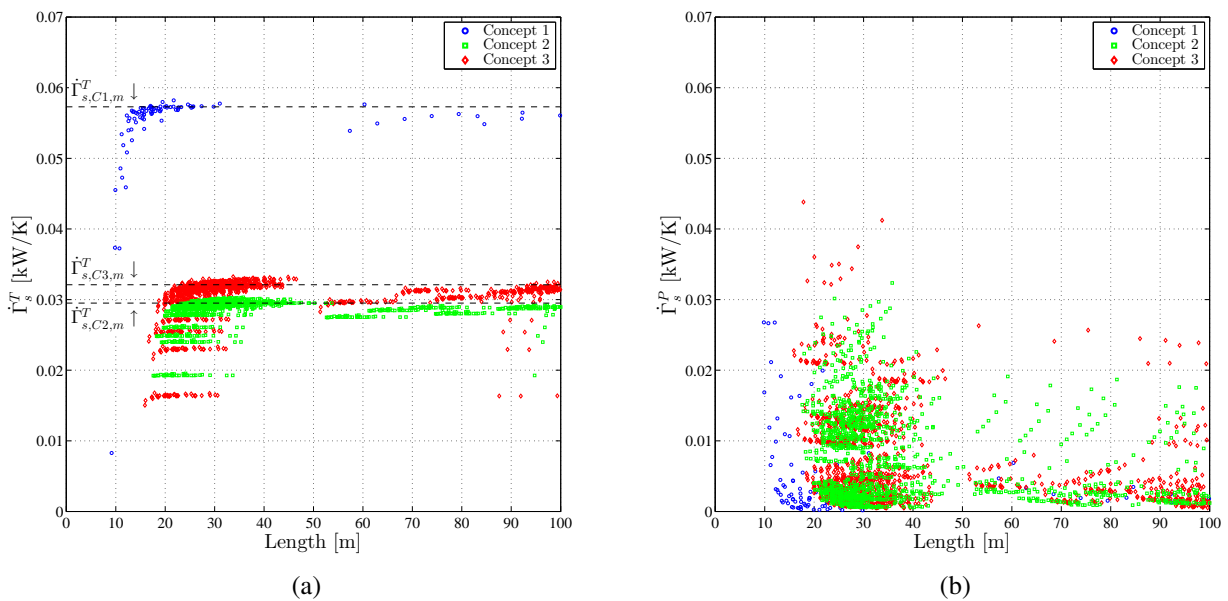

(a)   (b)

Fig. 6. Thermally driven (a) and pressure driven (b) entropy generation rate and total tube length for all feasible solution of concept 1, 2 and 3.

and lowest for concept 2, as also suggested by figure 5a. From figure 6b it is seen that, for all lengths a combination exists that diminishes the contribution from pressure driven entropy generation. It is also seen that a range of combinations exists that results in a large contribution from pressure driven irreversibilities. This suggests that the applied method, of first minimizing thermal entropy generation and then designing to minimize total entropy, is a valid approach.

Figure 7 shows a close up of the pareto frontier of concept 1 near the point $(L_m, \dot{\Gamma}_{s,m})$. It is seen that the feasible solution closest to the this point is the two circuit evaporator, $N = 2$, with a DN20 hydrogen pipe and a DN50 refrigerant pipe. For this solution the total length is $L = 12.6$m and the total entropy generation rate is $\dot{\Gamma}_s = 0.0583$kW/K.

Since there is no restriction on the combination of circuit and pipe sizes between the low and high-stages of concept 2 and 3 it can be assumed that the points that compile the pareto frontier in figure 5b are the sum of the points on the pareto frontier of the high and low-stage separately. The optimal solution for the high and low-stage of concept 2 and 3 is therefore found by the same procedure as seen in figure 7.

The optimal solution for all three concepts are presented in table 3. Here the necessary tube length is also seen. Concept 1 yields the shortest length of 12.6m while concept 2 is the longest with 20.1m, thus an increase in size of 59% compared to concept 1. Concept 3 has a length of 18.4m, 46% longer than concept 1. Further it is seen that there is no significant difference between the total length of the low and high-stage of concept 2 and 3.

The entropy generation rates for the optimal solutions for all three concepts are presented in 4. The thermal and pressure driven contributions are also presented. Further, the ratio f, which is the components share of the total entropy generation rate is shown. It is seen that the thermally driven part is between 82-95% and is thus the main contributor to the total entropy generation rate. Further it can be seen that the main reduction of entropy generation, attained by concept 2 and 3 is achieved by a reduction of thermal entropy generation.
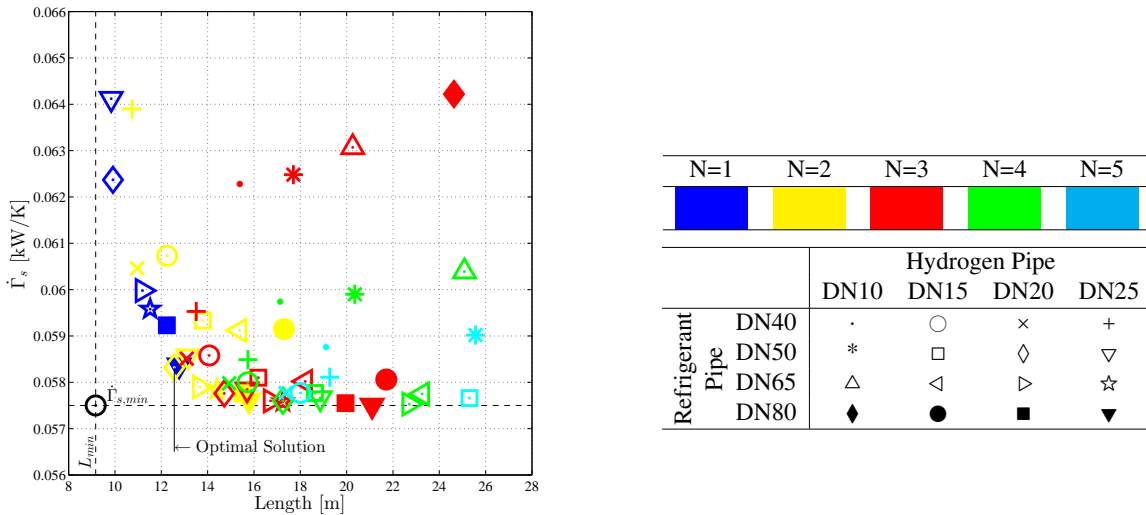
Fig. 7. Close up view of the pareto frontier for concept 1 close to the point $(L_{min}, \dot{\Gamma}_{s,min})$.

Table 3. Optimal refrigerant pipe size (RPS), hydrogen pipe size (HPS), circuit number and resulting total length for concept 1, 2 and 3

	Low-stage				High-stage				Total
	HPS$_{opt,L}$	RPS$_{opt,L}$	$N_{opt,L}$	$L_{opt,L}$	HPS$_{opt,H}$	RPS$_{opt,H}$	$N_{opt,H}$	$L_{opt,H}$	$L_{opt,tot}$
Concept 1	DN20	DN50	2	12.6m	-	-	-	-	12.6m
Concept 2	DN25	DN50	1	9.38m	DN25	DN50	1	10.8m	20.1m
Concept 3	DN25	DN50	1	9.46m	DN25	DN40	1	8.98m	18.4m

Table 4. Thermal and pressure driven entropy generation rate for the optimal solution of concept 1, 2 and 3. n is the value and f is components share of the total entropy generation

		Low-stage		High-stage		Total	
		n [kW/K]	f [-]	n [kW/K]	f [-]	n [kW/K]	f [-]
Concept 1	$\dot{\Gamma}_s^T$	-	-	-	-	0.0552	0.95
	$\dot{\Gamma}_s^P$	-	-	-	-	0.0031	0.05
	$\dot{\Gamma}_s$	-	-	-	-	0.0583	-
Concept 2	$\dot{\Gamma}_s^T$	0.0132	0.83	0.0145	0.97	0.0277	0.90
	$\dot{\Gamma}_s^P$	0.0026	0.17	0.0005	0.03	0.0031	0.10
	$\dot{\Gamma}_s$	0.0158	-	0.0150	-	0.0308	-
Concept 3	$\dot{\Gamma}_s^T$	0.0156	0.82	0.0128	0.87	0.0284	0.84
	$\dot{\Gamma}_s^P$	0.0035	0.18	0.0019	0.13	0.0054	0.16
	$\dot{\Gamma}_s$	0.0191	-	0.0147	-	0.0338	-

4 Conclusion

This has studied three different concepts for cooling hydrogen at hydrogen refuelling stations in accordance with SAE-J2601. This demands that hydrogen is cooled to -40°C under the duration of the refuelling. The dimensioning conditions where an ambient temperature of 30°C and a cooling load of 72kW.

For minimizing the thermal entropy generation, concept 2 showed the highest potential, reducing the entropy generation rate by 47% compared concept 1. This was attained with an intermediate hydrogen temperature of 4°C and 55% of the load supplied by the high-stage evaporator. Concept 3 reduced the entropy generation rate by 42%. This with an intermediate hydrogen temperature of -17°C and 49% of the load supplied by the high-stage.

A zero-dimensional numerical heat transfer model of a tube in tube evaporator has been built and was used to dimension the evaporators according to the dimensioning conditions and the optimal intermediate hydrogen temperature. All feasible solutions where found for combinations of a range of commercially available pipes. The feasible solutions were found to be limited by a pareto frontier. From the pareto frontier the optimal solution was defined as the point closest to the intersection of the pareto frontier's vertical and horizontal asymptote.

For concept 1 this was a two circuit evaporator, N =2, with a DN20 hydrogen pipe and a DN50 refrigerant pipe. This resulted in a total length of L =12.6m and a total entropy generation rate of $\dot{\Gamma}_s$ =0.0583kW/K.

For concept 2 the optimal solution for both the high and low-stage was a one circuit evaporator, N =1, with a DN25 hydrogen pipe and a DN50 refrigerant pipe. Which lead to a total tube length of L = 20.1m and a total entropy generation rate of $\dot{\Gamma}_s$ =0.0308kW/K.

The optimal solution for the high-stage evaporator of concept 3 was a one circuit evaporator, N =1, with a DN25 hydrogen pipe and DN40 refrigerant pipe. For the low-stage it was a one circuit evaporator, N =1, with a DN25 hydrogen pipe and DN50 refrigerant pipe. The total tube length for concept 3 was the L =18.4m and the total entropy generation rate was $\dot{\Gamma}_s$ =0.0338kW/K.

It was found that the main contribution to the irreversibilities for the optimal solutions was the thermally driven entropy generation. The contribution from fluid flow was in the order of 5-16%. This suggest the that method of first minimizing thermal entropy generation and then dimensioning the evaporator to the reduce the contribution from fluid flow is valid.

In conclusion concept 2 showed the highest potential for reducing entropy generation with a reduction of 49% compared to concept 1 and 9% compared to option 3. This reduction of entropy generation was attained by increasing the total tube length with by 59% compared to concept 1. Concept 3 offers a lower reduction of entropy generation but still necessitates an increase in tube length of 46% and was thus not found to be favourable solution.

Nomenclature

Abbreviations

APRR   Average Pressure Ramp Rate
COP   Coefficient Of Performance
EES   Engineering Equation Solver
HPS   Hydrogen Pipe Size
NPS   Nominal Pipe Size
RPS   Refrigerant Pipe Size

Subscripts

$C1$ Hydrogen cooling concept 1
$C2$ Hydrogen cooling concept 2
$C3$ Hydrogen cooling concept 3
c Circuit
hyd Hydrogen
H High stage evaporator
in Flow into control volume
i Inner
L Low stage evaporator
M Mechanical
m Minimum
opt Optimal
out Flow out of control volume
o Outer
ref Refrigerant
tot Total

Superscripts

P Pressure driven entropy generation
T Thermally driven entropy generation

Symbols

$\bar{\alpha}$	Average Heat Transfer Coefficient	kW/m²-K
$\dot{\Gamma}_s$	Entropy Generation Rate	kW/K
$\dot{m}$	Mass Flow Rate	kg/s
$\dot{Q}$	Heat Load	kW
ϵ	Absolute Roughness	m
A	Area	m²
D	Diameter	m
f	Share of thermal or pressure driven entropy generation to the total	-
h	Specific Enthalpy	kj/kg
k	Conductivity	kW/m-K
L	Length	m
LS	High Stage Load Share	-
N	Number of Tube in Tube Circuits	-
r	Real Roughness of Pipe	-
s	Specific Entropy	kj/kg-K
t	Pipe Wall Thickness	m
UA	Over All Heat Transfer Coefficient	kW/m²-K
x	Vapour Mass Fraction (Vapour Quality)	-

References

[1] Liu YL, Zhao YZ, Zhao L, Li X, gang Chen H, Zhang LF, et al. Experimental studies on temperature rise within a hydrogen cylinder during refueling. International Journal of Hydrogen Energy. 2010;35(7):2627 – 2632.

[2] Zhao L, Liu Y, Yang J, Zhao Y, Zheng J, Bie H, et al. Numerical simulation of temperature rise within hydrogen vehicle cylinder during refueling. International Journal of Hydrogen Energy. 2010;35(15):8092 – 8100.

[3] Dicken CJB, Mérida W. Measured effects of filling time and initial mass on the temperature distribution within a hydrogen cylinder during refuelling. Journal of Power Sources. 2007;165(1):324 – 336.

[4] Galassi MC, Baraldi D, Iborra BA, Moretto P. CFD analysis of fast filling scenarios for 70 MPa hydrogen type IV tanks. International Journal of Hydrogen Energy. 2012;37(8):6886 – 6892.

[5] SAE-International. Fueling Protocol for Light Duty Gaseous Hydrogen Surface Vehicles. SAE International;.

[6] Morosuk T, Tsatsaronis G. Advanced Exergetic Evaluation of Refrigeration Machines Using Different Working Fluids. Energy. 2009 Dec;34(12):2248–2258.

[7] Granryd E. Refrigerating Engineering. Royal Institute of Technology, KTH, Department of Energy Technology, Division of Applied Thermodynamics and Refrigeration; 2009.

[8] Jensen JK. Thermodynamic and Thermoeconomic Analysis of Refrigeration Systems for Hydrogen Refueling Stations. Technical University of Denmark, Department of Mechanical Engineering; 2012.

[9] Bejan A, Tsatsaronis G, Moran MJ. Thermal Design and Optimization. Wiley-Interscience publication. Wiley; 1996.

[10] Klein SA. Engineering Equation Solver Academic Professional V9.170; 2012.

[11] Shah MM. Chart correlation for saturated boiling heat transfer: equations and further study. ASHRAE Transactions. 1982;88, part 1.:185–196.

[12] Didi MBO, Kattan N, Thome JR. Prediction of Two-Phase Pressure Gradients of Refrigerants in Horizontal Tubes. International Journal of Refrigeration. 2002;Vol 25:935–947.

[13] Müller-Steinhagen H, Heck K. A simple friction pressure drop correlation for two-phase flow in pipes. Chemical Engineering and Processing: Process Intensification. 1986;20(6):297 – 308.

[14] Shah RK, London AL. Laminar Flow Forced Convection in Ducts. Academic Press. 1978;.

[15] Chilton TH, Colburn AP. Mass Transfer (Absorption) Coefficients Prediction from Data on Heat Transfer and Fluid Friction. Industrial & Engineering Chemistry. 1934;26(11):1183–1187.

[16] Churchill SW. Friction-Factor Equation Spans All Fluid-Flow Regimes. Chemical Engineering. 1977;84(24):91–92.

[17] Zigrang DJ, Sylvester ND. Explicit approximations to the solution of Colebrook's friction factor equation. AIChE Journal. 1982;Vol 28:514–515.

[18] of Mechanical Engineers AS. Welded and Seamless Wrought Steel Pipes. ASME B3610M-2004. 2004;.